Constraining Scalar-Tensor Beyond-GR Theories

Rafeh Rehan
University of Toronto
(Dated: August 25, 2022)

We propose model independent parameterizations of scalar fields for Scalar-tensor theories in which the extra force is screened by Ratra-Peebles Chameleon and Symmetron screening. The effect of this parameterization is calculated on the luminosity, flux, and temperature of a thin accretion disk surrounding a spherically symmetric black hole. Perturbations to the geometry caused by matter and the field are not considered. Nonetheless, we show shadow deformations for perturbed geometries.

I. INTRODUCTION

Einstein's theory of General Relativity is an incredible success. Along with quantum mechanics, it revolutionized the state of physics in the early 20^{th} century. GR has predicted the deflection of light, the precession of perihelia, gravitational redshift, and gravitational waves, all of which have been confirmed experimentally with great precision [1][2].

Although it is the best theory of gravity we have, GR is incomplete. At cosmological scales, dark matter is required to explain galactic rotation curves, however it remains undetected. Dark energy is also posited to drive the expansion of the universe, causing the observed galactic redshifts, and many questions still surround it [3]. Singularities in GR are unavoidable, and there are fundamental problems when trying to extend GR to the quantum domain [4][1].

Alternative theories of gravity attempt to solve some of these problems through several different strategies. $f(R)$ theories of gravity consider higher order derivatives of the metric, while Scalar-tensor theories add additional fields to the Einstein-Hilbert action. This paper focuses on Scalar-tensor theories of gravity. It is important to note, since Solar System tests of GR agree well with the theory, the effect of extra fields in Scalar-tensor theories need to be negligible locally, while significantly deviating on cosmological scales [5].

In Scalar-tensor theories, the profile of these additional fields determine how they affect surrounding matter distributions. Recently, we have learned that field profiles subject to Ratra-Peebles Chameleon and Symmetron screening mechanisms can be characterized by smooth step-like functions with varying tail lengths [6].

In this paper, we propose two model independent spherically symmetric parameterizations of scalar fields in Scalar-tensor theories motivated by the work done in [6]. Both parameterizations represent scalar fields screened by Ratra-Peebles Chameleon and Symmetron mechanisms. Both models exhibit step-like behaviour and differ by the length of their tails.

Since these additional fields contribute to gravitational interactions, one can observe their interaction with matter particles. This will be done by calculating the changes in luminosity, flux, and temperature of a thin accretion disk surrounding a spherically symmetric black hole.

The considered system consists of a Schwarzschild black hole, a radially symmetric scalar field, and matter distribution. For a self-consistent analysis, the perturbative effects on the space-time geometry due to the field and matter should be considered, but are not in this work. Although these effects are not considered, we show shadow deformations caused by geometrical perturbations away from the Schwarzschild solution. This is done in Appendix A.

In Section II the dynamics of massive particles in the Schwarzschild geometry are analyzed to establish a basis of reference. In Section III, the model independent parameterizations of scalar fields in Scalar-tensor theories being considered are developed. Space-time geometries conformally related to the Schwarzschild solution are also analyzed. Section IV develops the machinery required to study the properties of thin accretion disks in each space-time geometry. In Section V, the effects of our parameterized scalar fields on the properties of thin accretion disks will be analyzed using a thin accretion disk in the Schwarzschild geometry for reference. Throughout, the metric signature $(-,+,+,+)$ is adopted.

II. MASSIVE PARTICLES IN THE SCHWARZSCHILD GEOMETRY

Accretion disks around a Schwarzschild black hole consist of massive particles travelling along geodesics of the Schwarzschild geometry. To analyze the properties of this accretion disk, the dynamics of massive particles in this space-time geometry are studied. The Lagrangian for a particle is given by

$$\begin{aligned} 2\mathcal{L} &= g_{\mu\nu}\dot{x^\mu}\dot{x^\nu} \\ &= g_{tt}\dot{t}^2 + g_{rr}\dot{r}^2 + r^2\left(\dot{\theta}^2 + \sin^2\theta\dot{\varphi}^2\right) \end{aligned} \tag{1}$$

where dot denotes derivatives with respect to the proper time τ for massive particles. In the Schwarzschild metric,

$$g_{tt} = -\frac{1}{g_{rr}} = -\left(1 - \frac{2M}{r}\right)$$

using $G = c = 1$.

In thin disk accretion, the height of the disk is significantly smaller than its radial size. Hence, one can work in the equatorial plane and take $\theta = \pi/2$, $\dot{\theta} = 0$. The Lagrangian is independent of t and φ, so two conserved quantities are obtained

$$E = -g_{tt}\dot{t} \tag{2}$$

$$L = r^2\dot{\varphi}. \tag{3}$$

For massive particles, E and L are the energy and angular momentum per particle respectively. In the adopted metric signature for massive particles, $\mathcal{L} = -1/2$. Rewriting (1) using our conserved quantities,

$$\dot{r}^2 + V_{\text{eff}}(r) = 0 \tag{4}$$

where V_{eff} is the effective potential defined as

$$V_{\text{eff}}(r) \equiv -g_{tt}\left(\frac{L^2}{r^2} + 1\right) - E^2. \tag{5}$$

For motion in a thin accretion disk, circular orbits with $\dot{r} = \ddot{r} = 0$ are of interest. Using (4), the necessary conditions for circular orbits are

$$V_{\text{eff}}(r) = 0, \frac{dV_{\text{eff}}}{dr} = 0. \tag{6}$$

From this, expressions for E and L in terms of the derivatives of the metric and the radial coordinate can be obtained

$$E = \left[\frac{2g_{tt}^2}{r\cdot\partial_r g_{tt} - 2g_{tt}}\right]^{1/2} \tag{7}$$

$$L = r\left[\frac{\partial_r g_{tt}}{2g_{tt}/r - \partial_r g_{tt}}\right]^{1/2}. \tag{8}$$

The angular velocity for a massive particle can be found using equations (2) and (3)

$$\Omega = \frac{d\varphi}{dt} = \frac{\dot{\varphi}}{\dot{t}} = -\frac{g_{tt}}{r^2}\frac{L}{E} \tag{9}$$

III. CONFORMAL TRANSFORMATIONS OF THE SCHWARZSCHILD GEOMETRY

To analyze the effect of static scalar Chameleon and Symmetron fields $\phi(r)$ in Scalar-tensor theories computed in [6], we consider conformal transformations of the form $\tilde{g}_{\mu\nu} = f(\phi)g_{\mu\nu}$. The forms of $\phi(r)$ are motivated by observing static scalar profiles for Chameleon and Symmetron screening mechanisms in [6]. Explicitly, we take a general logistic model with a parameterized height a and width b in the Einstein frame,

$$\phi_{logistic}(r) = \frac{a}{1 + e^{b(r-r_0)}}. \tag{10}$$

This model has a short tail, so to cover cases of scalar profiles with long tails, we consider a piecewise lorentzian scalar profile

$$\phi_{textlorentz}(r) = \begin{cases} a & r < 0 \\ \frac{a}{1+(r/\lambda)^2} & r \geq 0. \end{cases} \tag{11}$$

Two forms of coupling to the metric will be considered. A quadratic and exponential coupling allowing us to analyze the effect of a Symmetron and Chameleon field respectively:

$$f_{\text{sym}}(\phi) = 1 + \frac{\phi^2}{\alpha^2} \tag{12}$$

$$f_{\text{chm}}(\phi) = \exp(\gamma\phi), \tag{13}$$

with coupling constants α and γ. Under a conformal transformation, the metric changes. Hence, new conserved quantities for a conformally related metric are obtained

$$\tilde{E} = -f(\phi)g_{tt}\dot{t} \tag{14}$$

$$\tilde{L} = f(\phi)r^2\dot{\varphi}. \tag{15}$$

Rewriting the Lagrangian for a conformally transformed metric,

$$\dot{r}^2 + \tilde{V}_{\text{eff}}(r) = 0 \tag{16}$$

with a new effective potential defining the trajectories of massive particles

$$\tilde{V}_{\text{eff}}(r) \equiv -\frac{g_{tt}}{f(\phi)}\left(\frac{\tilde{L}^2}{f(\phi)r^2} + 1\right) - \frac{\tilde{E}^2}{f^2(\phi)}. \tag{17}$$

The same treatment of imposing the conditions for circular orbits allows one to obtain similar expressions for the energy and angular momentum per massive particle

$$\tilde{E} = \left[\frac{g_{tt}^2(2f + f'r)}{r\cdot\partial_r g_{tt} - 2g_{tt}}\right]^{1/2} \tag{18}$$

$$\tilde{L} = r\left[\frac{\partial_r g_{tt}\cdot f + g_{tt}f'}{2g_{tt}/r - \partial_r g_{tt}}\right]^{1/2}, \tag{19}$$

where prime denotes the derivative with respect to r. Notice that if one takes $f(\phi) = 1$ the equations (7) and (8) for the Schwarzschild geometry are recovered as expected. The angular velocity in this conformally related geometry is unchanged.

IV. THIN DISK ACCRETION

In this section, the expressions for flux, temperature, and luminosity in the thin disk accretion model are specified. The flux of the disk in the thin disk accretion model is derived in [7]. It is given by

$$F(r) = -\frac{\dot{M}}{4\pi\sqrt{-g}}\frac{\partial_r\Omega}{(E - \Omega L)^2}\int_{r_{isco}}^{r}(E - \Omega L)\partial_r L dr, \tag{20}$$

where $\dot{M}$ is the constant accretion rate and g is the determinant of the metric. r_{isco} is the radius of innermost stable circular orbit and can be found by finding the zeros of the second derivative of the effective potential. This radius acts as the beginning of our accretion disk.

Treating the accretion disk as a black body, the temperature of the disk is related to its flux by the Stefan-Boltzmann law

$$T(r) = \left(\frac{F(r)}{\sigma}\right)^{1/4}, \tag{21}$$

where σ is the Stefan-Boltzmann constant.

The expression for the luminosity of the disk is also derived in [7]. It is given to be

$$L(\nu) = 8\pi h \cos(i) \int_0^{2\pi} \int_{r_{isco}}^{r_{disk}} \frac{\nu^3 d\varphi dr}{\exp\left(h\nu_e/k_b T\right) - 1}, \tag{22}$$

where k_b is the Boltzmann constant and i is the inclination angle (which we take to be 0). The observed frequency ν is related to the emitted frequency ν_e by the redshift factor. For the conformally related geometries, this is given by

$$\tilde{g}_z = \frac{\nu}{\nu_e} = \frac{E_o}{E_e} = \frac{\tilde{g}_{\mu\nu} p^\nu u_o^\mu}{\tilde{g}_{\mu\nu} p^\nu u_e^\mu} \tag{23}$$

where E_o and E_e is the energy of a particle in the observer's and particle's frame respectively. p^μ is the 4-momentum of the particle in the observer's frame and u^μ is it's frame dependent 4-velocity. From [7], the 4-velocity in the observer's frame is $u_o^\mu = (1, 0, 0, 0)$, and in the emitted frame $u_e^\mu = u_e^t(1, 0, 0, \Omega)$. The 4-momentum in the particle's reference frame is $p^\nu = (\dot{t}, 0, 0, \dot{\varphi})$. u_e^t can be found from the timelike normalization condition $\tilde{g}_{\mu\nu} u_e^\mu u_e^\nu = -1$ which gives

$$\tilde{g}_z = \frac{\sqrt{-f\left(g_{tt} + g_{\varphi\varphi}\Omega^2\right)}}{1 - \tilde{L}\Omega/\tilde{E}}. \tag{24}$$

One can recover the redshift factor for the Schwarzschild geometry by setting $f(\phi) = 1$ and taking $\tilde{L}, \tilde{E} \to L, E$.

V. RESULTS

In this section, the flux, temperature, and luminosity distributions obtained in the Schwarzschild geometry are compared to the conformally related geometries. The conformally related geometries are specified by the two different forms of conformal factors (12) and (13) and scalar field parameterizations (10) and (11).

We define a new quantity to parameterize our results, the penetration radius r_p defined as follows. Let ϕ^* be the screened value of the field, taken for our purposes to be 10^{-3}. If at some radius, $\phi(r^*) = \phi^*$, then $r_p \equiv r^* - r_{isco}$. That is, the penetration radius r_p is how far the field gets through the accretion disk before becoming screened.

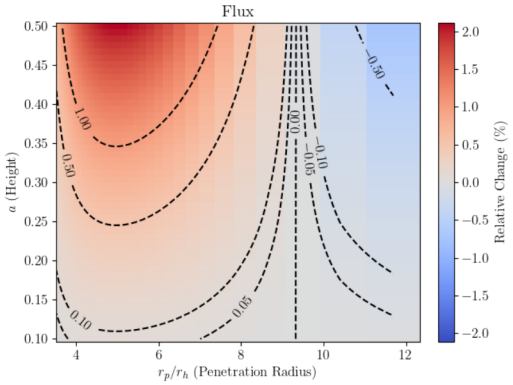

FIG. 1. Relative percent differences of Flux for $\phi_{\text{logistic}}(r)$ model parameterization with conformal factor $f_{\text{sym}}(\phi)$. $\alpha^2 = 80$.

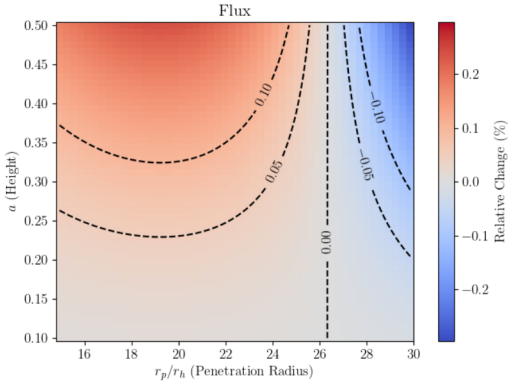

FIG. 2. Relative percent differences of Flux for $\phi_{\text{lorentz}}(r)$ model parameterization with conformal factor $f_{\text{sym}}(\phi)$. $\alpha^2 = 80$.

The penetration radius was found using a FORTRAN implementation of Newton's root finding algorithm [8].

In Figures 1-8, we plot the relative percent differences between the peaks of the distributions of flux, temperature, and luminosity as functions of a and r_p for different values of coupling constants α and γ. The integration in equations (20) and (22) were done numerically in FORTRAN using Simpson's 3/8 rule [8]. 50 values of both parameters a and r_p were chosen for a total of 2500 different field configurations per graph. We assume a thin accretion disk surrounding a supermassive Schwarzschild black hole with $M = 10^9 M_\odot$ and a constant accretion rate of $\dot{M} = 1 M_\odot/yr$.

Values for the coupling constants were chosen to keep the scalar fields "light". This corresponds to values of α and γ such that $a \ll \alpha$ and $a \ll 1/\gamma$. We also include plots showing the relative percent differences between the radii of peak temperatures of the disk.

Contour lines are drawn for relative percent differences at and below the 1% level. These indicate regions of the parameter space where these scalar field models produce differences to GR that fit within error bars of current measurements. These plots give a sense of the order of

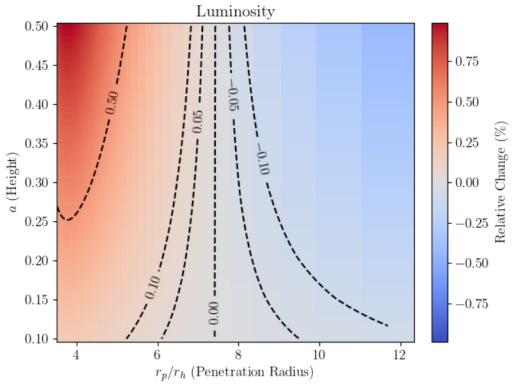

FIG. 3. Relative percent differences of Luminosity for $\phi_{\text{logistic}}(r)$ model parameterization with conformal factor $f_{\text{chm}}(\phi)$. $\gamma = 0.005$.

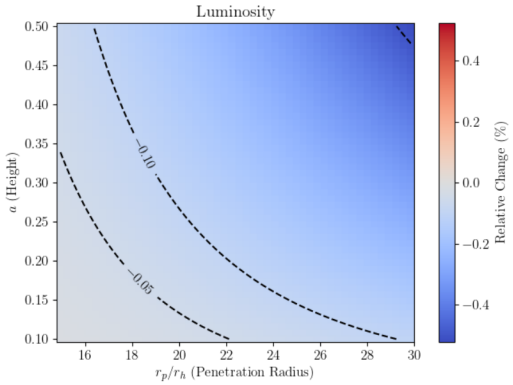

FIG. 4. Relative percent differences of Luminosity for $\phi_{\text{lorentz}}(r)$ model parameterization with conformal factor $f_{\text{chm}}(\phi)$. $\gamma = 0.005$.

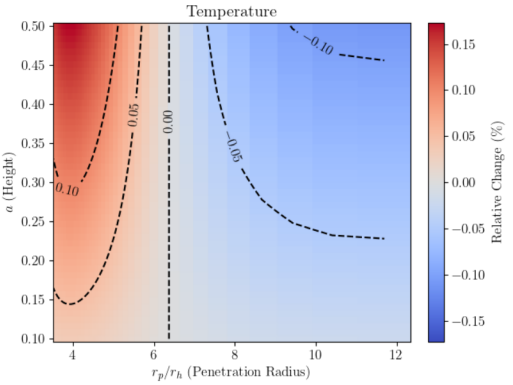

FIG. 5. Relative percent differences of Temperature for $\phi_{\text{logistic}}(r)$ model parameterization with conformal factor $f_{\text{chm}}(\phi)$. $\gamma = 0.001$.

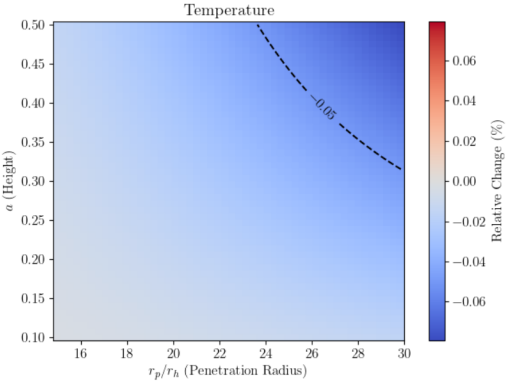

FIG. 6. Relative percent differences of Temperature for $\phi_{\text{lorentz}}(r)$ model parameterization with conformal factor $f_{\text{chm}}(\phi)$. $\gamma = 0.001$.

magnitude of effects of our model independent parameterization of scalar fields in Scalar-tensor theories on the properties of thin accretion disks. A self-consistent treatment of the effect of these parameterized scalar fields in Scalar-tensor theories on thin accretion disks would involve the consideration of a geometry perturbed away from the Schwarzschild solution. This could be done by treating the mass of the scalar field and matter in the accretion disk as perturbative effects to the Schwarzschild geometry. This would produce a new metric in which the resulting relative percent differences in luminosity, flux, and temperature would be more accurate. In this perturbed geometry, the geodesics of massless particles could also be studied. This would show changes to the shadow of a Schwarzschild black hole in Scalar-tensor theories considered in this paper.

Appendix A: Black Hole Shadows

Photon geodesics are not affected by conformal transformations. They can be studied by considering geometrical deformations sourced by accreting matter and the scalar field. Although this calculation is not within to the scope of our work, we devise a FORTRAN algorithm to draw black hole shadows by finding the minimal impact parameter needed for a photon to scatter around a black hole. The algorithm solves the geodesic equations using an implicit Runge-Kutta method with 10^{th} order Gauss-Legendre quadrature for the choice of coefficients. To illustrate the effect of geometries perturbed away from the Schwarzschild solution, we use a metric given in [9]. This metric is given by

$$ds^2 = -e^{\nu(r)}dt^2 + e^{\lambda(r)}dr^2 + r^2(d\theta^2 + \sin^2\theta d\varphi^2). \quad \text{(A1)}$$

where

$$e^{\nu(r)} = e^{-\lambda(r)} = 1 + \frac{3M}{\eta} - \frac{2M}{r} - \left(1 + \frac{6M}{\eta}\right)\left(\frac{r}{\eta}\right) + \left(\frac{r}{\eta}\right)^2 \left(1 + \left(1 + \frac{6M}{\eta}\right) \ln\left[A\left(1 + \frac{\eta}{r}\right)\right]\right) \quad \text{(A2)}$$

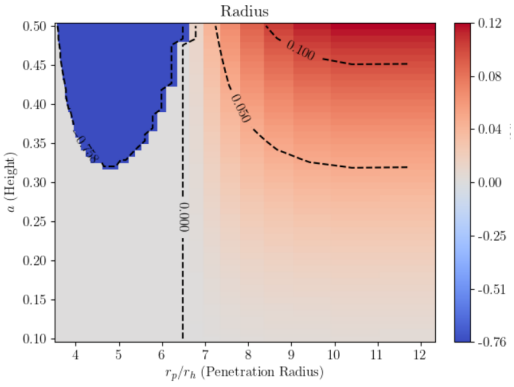

FIG. 7. Relative percent differences of peak energy emission radius for $\phi_{\text{logistic}}(r)$ model parameterization with conformal factor $f_{\text{sym}}(\phi)$. $\alpha = 80$.

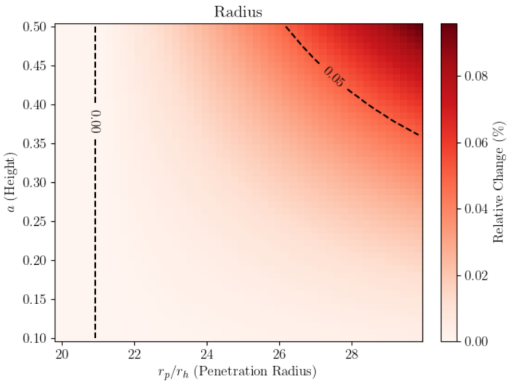

FIG. 8. Relative percent differences of peak energy emission radius for $\phi_{\text{lorentz}}(r)$ model parameterization with conformal factor $f_{\text{sym}}(\phi)$. $\alpha = 80$.

We plot the resulting shadows for different space-time geometries in Figure 9. α and β are sky coordinates given in [10] and derived to be

$$\alpha = -r_0^2 \sin\theta_0 \frac{d\varphi}{dr}\Big|_{r_0} \tag{A3}$$

$$\beta = r_0^2 \frac{d\theta}{dr}\Big|_{r_0}, \tag{A4}$$

where r_0 and θ_0 are the radius and polar angle of the observer respectively. For our calculations, $r_0 = 100GM/c^2$ and $\theta_0 = \pi/2$.

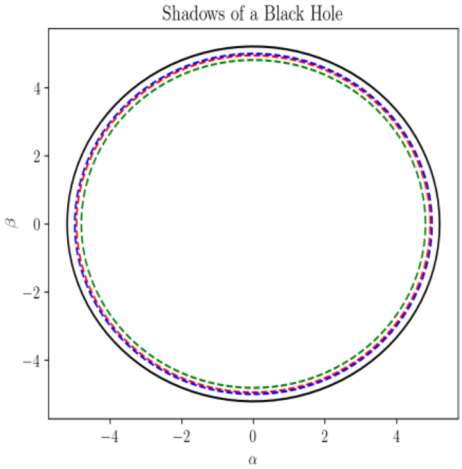

FIG. 9. Shadows of black holes in different geometries. The solid black line is the shadow of a Schwarzschild black hole for $r_0 = 100GM/c^2$, $\theta_0 = \pi/2$. Dashed lines show shadows of the metric in [9] for different model parameters. Red has $A = 3 \times 10^{-3}, \eta = M/A$. Blue has $A = -3 \times 10^{-3}, \eta = M/A$. Green has $A = 3 \times 10^{-3}, \eta = 3M/A$.

[1] S. Carroll, *Spacetime and Geometry: An Introduction to General Relativity* (Benjamin Cummings, 2003).

[2] C. M. Will, "The confrontation between general relativity and experiment," (2006).

[3] C. A. Sporea, "Notes on f(r) theories of gravity," (2014), arXiv:1403.3852 [gr-qc].

[4] L. Maccone, "A fundamental problem in quantizing general relativity," (2019).

[5] T. Clifton, P. G. Ferreira, A. Padilla, and C. Skordis, Physics Reports **513**, 1 (2012), modified Gravity and Cosmology.

[6] A. V. Frolov, J. T. Gálvez Ghersi, and A. Zucca, "Unscreening scalarons with a black hole," (2017).

[7] C. Liu, S. Yang, Q. Wu, and T. Zhu, Journal of Cosmology and Astroparticle Physics **2022**, 034 (2022).

[8] K. E. Atkinson, *An Introduction to Numerical Analysis*, 2nd ed. (John Wiley & Sons, New York, 1989).

[9] C. S. J. Pun, Z. Kovács, and T. Harko, Physical Review D **78** (2008), 10.1103/physrevd.78.024043.

[10] S. Vázquez and E. Esteban, Il Nuovo Cimento B **119**, 489–519 (2004).